Fracture Tolerance Related to Skeletal Development and Aging Throughout Life: 3-Point Bending of Human Femurs

Jason L. Forman[1, 2], Eduardo del Pozo de Dios[2], Ioannis Symeonidis[3], Julio Duart[4], Jason R. Kerrigan[1], Robert S. Salzar[1], Sriram Balasubramanian[5], Maria Segui-Gomez[2], Richard W. Kent[1]

Abstract This study investigated the mechanical factors contributing to changes in fracture tolerance of the femur throughout skeletal development, maturity and advanced age. A database was compiled from the literature describing dynamic three-point bending tolerances of cadaver femurs. This database was augmented with 23 new tests targeting pediatric and young adult ages (median age of new tests: 27 years). For a subset of specimens an analytical model was developed to decompose the observed changes with age into contributing geometric and material factors. The resulting aggregated dataset included tests on 83 specimens, with an age range of 16 months to 83 years. The fracture moments ranged from 20 Nm (for a pediatric specimen) to 630 Nm (for an adult male). The data showed a rapid increase in fracture moment during skeletal development with a plateau or peak during adulthood (approximately 25-45 years). This was followed by a general decrease in fracture moment in advanced age. Decomposition of these trends suggests that the increase in strength through skeletal development was attributable to geometric changes. The decrease in fracture moment in advanced age was likely due to decreases in cortical thickness combined with other factors, possibly including a decrease in cortical bone ultimate stress.

Keywords Aging, femur, fracture, pediatric, development

I. INTRODUCTION

There are several geometric and material changes that occur throughout development and aging that may affect skeletal injury tolerance. The physical size of the skeleton grows throughout development, including both increasing length, cross-sectional area, and cortical bone thickness [1], [2]. The material characteristics of cortical bone change, including decreasing ultimate stress and strain in advanced age [3], [4]. The microscopic morphology of the bone also changes, often resulting in increasing porosity [5], [6], [7], [8] and decreased fracture toughness [9], [10], [11] with advanced age.

To understand the relation between age and injury tolerance, it is desirable to know how injury tolerance relates to the mechanical changes that occur in the skeleton with age. Several studies have investigated the mechanisms of changes in skeletal injury tolerance either for the elderly (e.g. [12], [13]) or for pediatric subjects (e.g. [14], [15]) for certain body regions. While those studies have provided valuable information, none have yet studied how the roles of contributing mechanistic factors change throughout the entire course of life.

The goal of this study was to investigate the roles of geometric and material factors in the changes that occur in long-bone fracture tolerance throughout skeletal development, adulthood and advanced age. Due to the large amount of information required, this study focused on a skeletal structure and injury mechanism for which a large amount of information is currently available: the femur subjected to dynamic, mid-shaft three-point bending. The first goal of this study was to compile a dataset (including new tests) describing femur bending tolerance throughout life (from very young to very old). The second goal was to study the contributing effects of changes in bone geometry and other characteristics via a component decomposition using a simplified beam model.

J. L. Forman is a Senior Scientist at the University of Virginia Center for Applied Biomechanics, with a Ph.D. in Mechanical Engineering (phone: +1 434 296 7288; fax: +1 434 296 3453; email: jlf3m@virginia.edu).
Author Affiliations: [1] University of Virginia Center for Applied Biomechanics; [2] European Center for Injury Prevention; [3] Institute for Legal Medicine, University of Munich; [4] Complejo Hospitalario de Navarra; [5] Children's Hospital of Philadelphia

II. METHODS

Existing Data

A database of dynamic femur bending tolerance experiments was compiled from information available in the open literature. The inclusion criteria were as follows:

- Part of a peer-reviewed study available in the open literature.
- Tests performed on whole human cadaveric femurs in three-point bending.
- The tests were performed such that the maximum bending moment was intended to occur in the mid-shaft of the femur.
- The tests were performed dynamically (loading applied at a rate of at least 500 mm/min).
- The results include a description of the maximum bending moment (assumed to be the fracture moment) calculated at the mid-shaft of the femur for each specimen.
- Ages included for each specimen.

Tests with either the superficial tissue (skin, muscle, etc.) removed or with the superficial tissue intact were included. Previous studies have indicated that, in general, the femur fracture moment tends to be insensitive to the direction of the applied load (e.g., applied in either the medial-lateral direction, or in the posterior-inferior direction [3]). Thus, in the main dataset, tests were included regardless of the direction of bending applied to the specimen.

New Experiments

New experiments were performed to augment the existing data, targeting specimen ages underrepresented in the literature. Following an initial examination of the literature, the target ages for new data collection ranged from very young (pediatric) to middle age (approximately 50 years).

Specimens were obtained through the Transplant and Tissue Donation Program of the Government of Navarra (Spain), of which the University of Navarra School of Medicine is a partner. All specimens were screened for blood-borne pathogens prior to inclusion in the study, and were stored by freezing until the time of preparation for testing. All tissue donation and handling procedures were approved by the University of Navarra School of Medicine.

Tests were performed with the same preparation and testing methods described by Kerrigan et al. [16]. Additional detail on the methods can be found therein. In brief, the specimens were prepared by first removing all of the superficial tissue and muscular attachments. Then, the proximal and distal ends of the specimens were encased (“potted”) in blocks of a two-part polymer material (FastCast, GoldenWest Manufacturing, Inc.). The specimens were oriented such that the bending moment would be applied about the anterior-posterior axis, with load applied to the mid-shaft of the femur in medial direction. The ends of the specimens were positioned in the polymer blocks such that the center of the head of the femur was co-linear with the center of the distal femoral notch (i.e., as a result, loading was applied perpendicular to a line drawn between the center of the femoral head and the femoral notch). The geometry of each specimen was documented after potting via a clinical computed tomography (CT) scan.

For testing, each of the potted ends of the specimens was attached to roller mounts (Figure 1). These rollers were then placed on supporting load cells (with a greased, smooth, plate interface). A bending moment was then applied via a loading ram (13 mm diameter) engaging the specimen at the mid-shaft, applying the load in the medial direction. This loading was applied by an Instron model 8874 material test machine. The ram was displaced with a target velocity of 1.5 m/s.

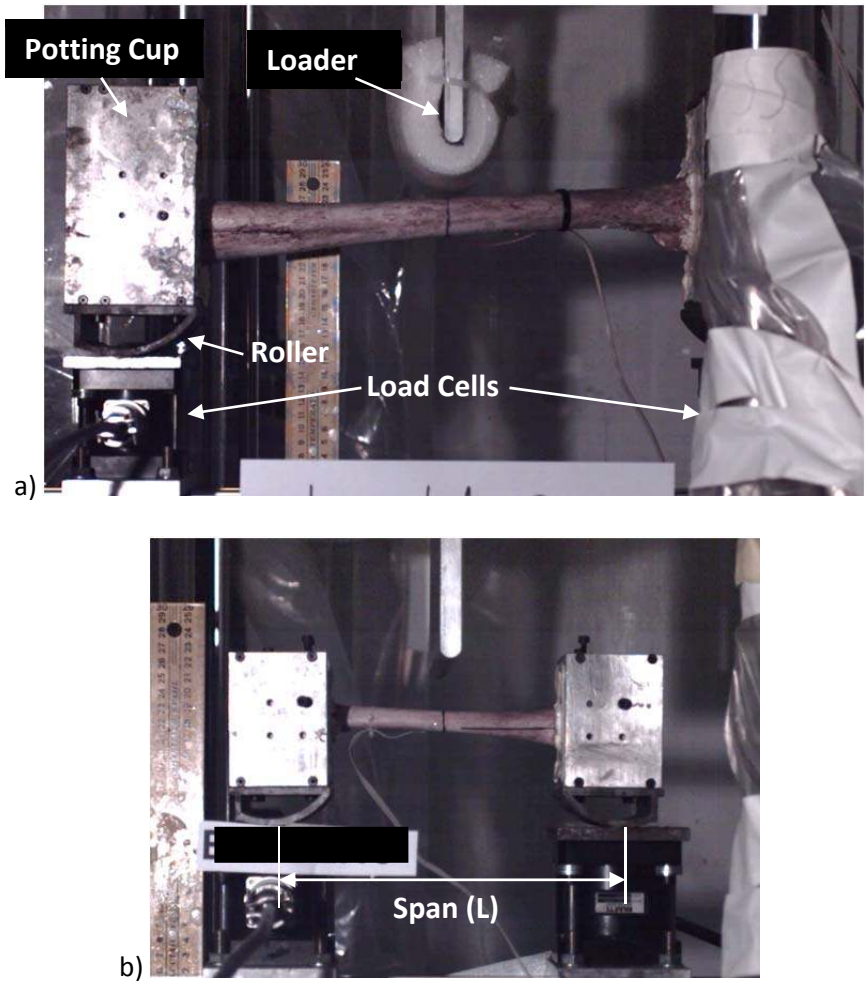

Figure 1: Video captures of an adult (top) and pediatric (bottom) specimen mounted in the test fixture prior to loading.

For the adult specimens, the geometry of the potting blocks and rollers were the same as those used by Kerrigan et al. [16]. For the smaller pediatric specimens, smaller potting blocks (7 cm by 7 cm by 50 cm thick) and rollers (44.5 mm radius) were used (Figure 1b). For the larger specimens, the loading ram was covered with closed-cell foam (approximately 25 mm thick) to limit local contact stresses. Due to limited space, this foam was removed for the smaller pediatric specimens.

Reaction loads were measured at the roller supports using 6-axis load cells (model MC3A, Advanced Mechanical Technology, Inc.). Data were collected at 10 kHz using a National Instruments Compact DAQ data acquisition system. All force and moment data were filtered with a Channel Frequency Class (CFC) 600 filter, per the recommended practices of the Society of Automotive Engineers standard J211 [17].

The mid-shaft moment, *M*, was calculated for each specimen:

$$M = \frac{L \times F_1 \times F_2}{F_1 + F_2} \quad (1)$$

Where *L* is the span and F_1 and F_2 are the vertical forces measured at the proximal and distal load cells.

As noted by Kerrigan et al. [16], the span, *L*, has the potential to change slightly during the test as the specimen flexes and the potting mounts rotate. To account for this, the locations of the center of contact (centers of pressure) between the load cell plates and the rollers were calculated at the time of peak load using the forces and moments measured by the load cells [16]. This loading location was combined with a measurement of the fixed span between the load cells to determine the specimen span used to calculate the peak mid-shaft moment. The mid-shaft moment at fracture moment was assumed to be the peak mid-shaft moment.

Cross-sectional geometric parameters were calculated at the mid-shaft of each specimen using the pre-test CT scans. For each specimen, cross-sectional contour lines outlining the geometry of the cortical bone were

generated for a CT slice taken from the mid-shaft, using Mimics (version 13, Materialise) CT analysis software, using threshold values chosen manually to achieve the best (qualitative) segmentation of the cortical bone. These contour lines were then imported into a computer aided design software package (SolidWorks 2011, SolidWorks Corp.) to calculate the cross-sectional area centroid, the cross-sectional area moment of inertia (I_{xx}; about a line passing through the centroid, perpendicular to the direction of loading), and the maximum distance from the centroid to the outer surface of the specimen parallel to the direction of loading (c_{max}).

Analysis

The specimen ages and fracture moments were compiled for the whole dataset. For the literature specimens tested with the superficial tissue intact, the peak moments were adjusted to account for the presence of the superficial tissue. Kerrigan et al. [16] found that removing the superficial tissue decreased the moment associated with a 50% risk of femur fracture by approximately 13.4%. This factor was assumed as an estimate of a scale factor to account for the presence of flesh. To implement this, the peak moments observed in the flesh-intact tests were multiplied by 0.866 to estimate the fracture moment that would be observed were those specimens denuded.

The goal of this study was to observe differences in femur moment tolerance across a life-span of ages, and to relate those differences to contributing mechanistic factors. Potential contributing factors were grouped into two overall categories: geometric factors and material factors. Consider an analytical model of mid-shaft 3-point bending of a simplified beam. If it is assumed that the neutral axis passes through the cross-sectional area centroid perpendicular to the direction of loading, then the bending moment is related to the peak longitudinal stress, σ_{max}, and cross-sectional geometry by the following:

$$M = \frac{I_{xx}\sigma_{max}}{c_{max}} \tag{2}$$

The moment at fracture, M_{fx}, may be similarly related to the ultimate stress, σ_{ult}, of the bone:

$$M_{fx} = \frac{I_{xx}\sigma_{ult}}{c_{max}} \tag{3}$$

The right-hand side of the equation can be grouped into factors relating to the cross-sectional geometry (I_{xx}/c_{max}, also known as the "section modulus") and a factor relating to the failure tolerance of the material (σ_{ult}).

$$M_{fx} = \left(\frac{I_{xx}}{c_{max}}\right) \times \sigma_{ult} \tag{4}$$

For the subset of specimens for which cross-sectional geometry information was available, mid-shaft I_{xx} and c_{max} were tabulated along with the specimen age and fracture moment. Due to the potential confounding effects of the cross-sectional orientation on I_{xx}, only the specimens tested in medial-lateral bending were used for this subset analysis. For each of those specimens, the peak moment was divided by the section modulus I_{xx}/c_{max} to calculate a remainder quantity (representing the mid-shaft moment at fracture normalized by the mid-shaft cross-sectional geometry). This normalized quantity may deviate somewhat from the true ultimate stress of the bone due to several confounding factors (e.g., shift of the neutral axis during loading, fracture initiating at a location other than the mid-shaft, etc.). As a result, it is not necessarily the intent of this study to represent this normalized value as an estimate of the ultimate stress of the bone. Instead, this normalized value will be referred to as variable S_{fx}, representing the mechanical factors other than the mid-shaft cross-sectional geometry that may contribute to fracture. This may include, but is not limited to, the ultimate stress of the tissue.

$$M_{fx} = \left(\frac{I_{xx}}{c_{max}}\right) \times S_{fx} \tag{5}$$

$$S_{fx} = {M_{fx}}\Big/{\left(\frac{I_{xx}}{c_{max}}\right)} \tag{6}$$

It was a goal to study and model how the geometric factors (I_{xx}/c_{max}) and the "other" factors (S_{fx}) change with age. The relationship between age and I_{xx}/c_{max} was modeled as quadratic, constrained to approach a value of

zero for zero age (Eq. 7). This form was chosen based on an initial examination of the data (via cross-plotting), and following an initial observance of an approximately linear relationship when the dependent variable, I_{xx}/c_{max}, was normalized by the independent variable, *Age* (Eq. 8).

$$\frac{I_{xx}}{c_{max}} = -a(Age)^2 + b(Age) \tag{7}$$

A preliminary analysis indicated that the residuals for this model would be approximately linearly dependent on age. This residual dependence on the independent variable would have violated assumptions inherent to the construction of prediction bounds for the model. To account for this, the data points and model were normalized by age:

$$\frac{I_{xx}}{c_{max} \times Age} = \frac{[-a(Age)^2 + b(Age)]}{Age} \tag{8}$$

The model coefficients *a* and *b* were determined through a least-squares fit based on the age-normalized values of I_{xx}/c_{max}. Model prediction bounds were calculated at a confidence level of 85%, chosen as the value that best qualitatively described the overall spread observed in the data. Note that prediction intervals differ from traditional model confidence intervals in that prediction intervals include random variations in the data to give uncertainty bounds for the prediction of new data points (in contrast, confidence intervals do not account for random variations in the data, but instead give uncertainty bounds for the potential path of the model). The model and prediction bounds were then de-normalized (multiplied by age) to plot against the de-normalized data.

A quadratic model was also chosen for S_{fx}. Previous studies have suggested that the ultimate stress of femur cortical bone subjected to uniaxial tension may be relatively consistent at least between ages 10-50. This is followed by a gradual decline with increasing age [3], [4]. To approximate this, the quadratic model chosen for S_{fx} was constrained to have a peak (zero slope) at zero age, resulting relatively little change in S_{fx} for the first 4-5 decades with a gradual decrease thereafter.

$$S_{fx} = d - c(Age)^2 \tag{9}$$

An initial analysis indicated that the residuals of the model in Equation 8 were independent of age. Thus, that model was fit directly to the data, without normalization. The model coefficients *c* and *d* were determined through a least-squares fit. Model prediction bounds were calculated with a 95% confidence level (again, chosen to achieve the best qualitative description of the range of the data).

These models were then combined to compare to a largermodel describing the relationship between fracture moment and age. Following Equation 5, a model for fracture moment versus age was generated by multiplying the model of I_{xx}/c_{max} (Eq. 7) with the model of S_{fx} (Eq. 8).:

$$M_{fx} = \left(\frac{I_{xx}}{c_{max}}\right) \times S_{fx} = [-a(Age)^2 + b(Age)] \times [d - c(Age)^2] \tag{10}$$

This was compared to a model of the same form, fit to the entire dataset.

$$M_{fx} = [-A(Age)^2 + B(Age)] \times [D - C(Age)^2] \tag{11}$$

Model coefficients *A*, *B*, *C* and *D* were determined through a least-squares fit of the fracture moment (versus age) data points of the whole dataset. This curve-fit was initiated with the values of *a*, *b*, *c*, and *d* as seed values for *A*, *B*, *C* and *D* (respectively). Prediction bounds were also calculated for this model with a confidence level of 95%.

III. RESULTS

Five studies were identified in the literature that met the inclusion criteria (Table I). These consisted of a combined 60 tests. Of those, 36 were medial-lateral bending tests that included information on the mid-shaft

cross-sectional geometry. The information and peak moment results for all of the identified tests are listed in Appendix A.

Twenty-three new tests were performed with specimen ages ranging from 1.3 to 57 years. The specimen information and peak moment results are shown in Appendix A. For one of those tests the CT scans failed, precluding the measurement of the cross-sectional geometry. This left 22 new tests which, when combined with the subset of previous tests, resulted in 58 medial-lateral bending tests for which detailed cross-sectional geometry was available. The resulting entire combined dataset consisted of 83 tests with specimens spanning ages from 1.3 years to 83 years.

TABLE I
PREVIOUS FEMUR BENDING STUDIES INCLUDED IN THIS ANALYSIS

Reference	Number of Tests	Age Range (years)	Typical Loading Rate (m/s)	Loading Direction*	Geometry Information?
Kennedy et al. 2004 [18]	25	49-83	5	M-L	Yes
Kerrigan et al. 2004 [16]	6	54-69	1.5	M-L	No
Funk et al. 2004 [19]	15	40-69	1.2	M-L and A-P	Yes
Kerrigan et al. 2003 [20]	4	54-59	1.5	M-L	Yes
Ouyang et al. 2003 [21]	10	2-12	0.008 (500 mm/min)	A-P	No

* M-L = medial-lateral bending; A-P = anterior-posterior bending

Figure 2 shows the peak moments (adjusted for the presence of flesh where necessary) plotted against specimen age for the entire dataset. Figure 3 shows the values of I_{xx}/c_{max} plotted against fracture moment for the subset of tests that were performed under medial-lateral bending and included information on the cross-sectional geometry. Figures 4a and 4b show the relationship between I_{xx}/c_{max} and age for that subset of specimens, including curve-fit models and prediction bounds. Figure 5 shows the relationship between the resulting remainder value, S_{fx}, and age for that subset (also with the corresponding model).

Figure 6 shows the fracture moments versus age for the entire dataset, with the combined subset model superimposed. For comparison this figure also includes the model described in Equation 11, generated from the entire dataset (with corresponding prediction bounds). The resulting coefficients for the subset model (Equation 10) and the entire dataset model (Equation 11) are shown in Table II.

IV. DISCUSSION

Fracture Moment

As shown in Figure 2, the fracture moments observed in the new tests were consistent with those observed in the previous studies. The entire combined dataset tended to show a relation between fracture moment and age rising steeply through adolescence with a peak or plateau between 25 and 50 years, followed by a decline with increasing age (Figure 2). These fracture moment ranges and trends are similar to previous studies. In a series of 604 dynamic bending tests with adult femurs, Kress et al. [22] observed fracture moments of approximately 100-600 Nm. In a series of 28 mid-shaft, dynamic, 4-point bending tests with adult femurs (age 47-83), Martens et al. [23] observed a mean fracture moment of 373 Nm. In a compilation of previous quasi-static test data, Yamada et al. [3] reported a decreasing trend in fracture moment from adulthood through advanced age (although the overall magnitudes of fracture moments in that study are low compared to the current study, likely due to a much slower loading rate).

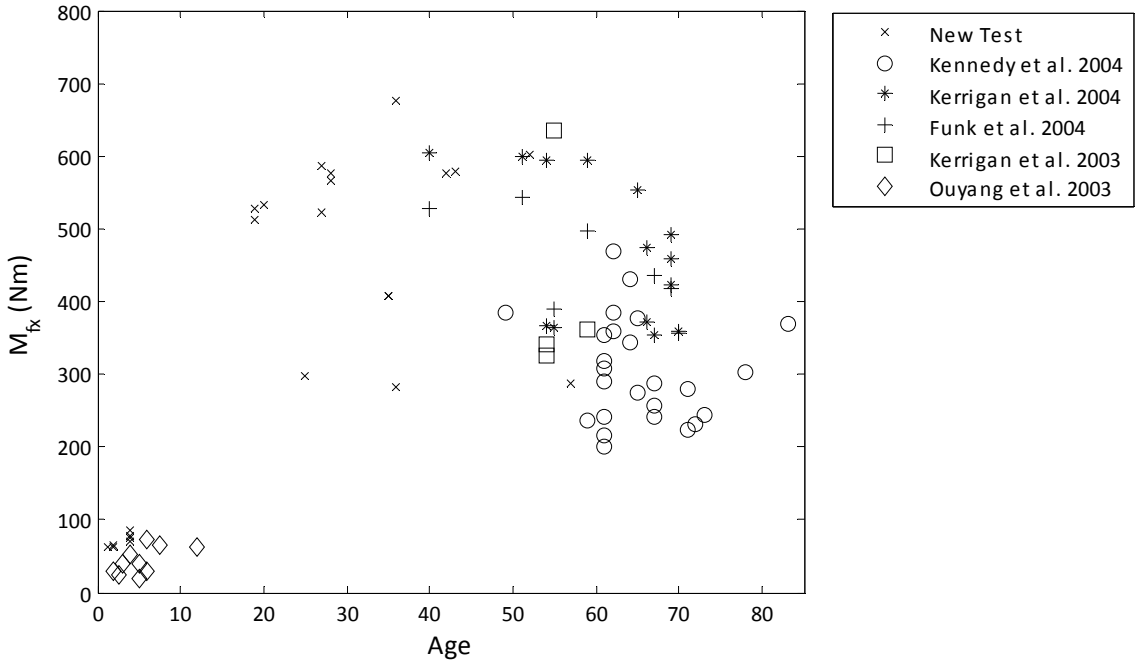

Figure 2: Mid-shaft femur bending moments at fracture, M_{fx}, versus age for the entire combined dataset. Data points marked by source (N=83 tests).

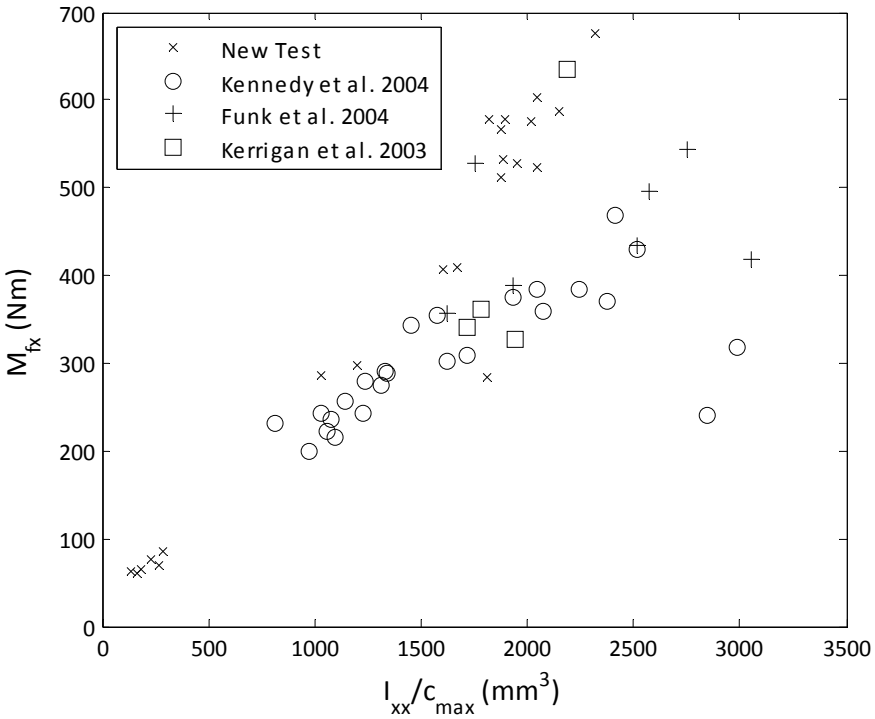

Figure 3: Fracture moments versus the section modulus, I_{xx}/c_{max}, measured at the mid shaft. Data shown are for the subset of tests performed in medial-lateral bending for which cross-sectional geometry information were available (n=58 tests).

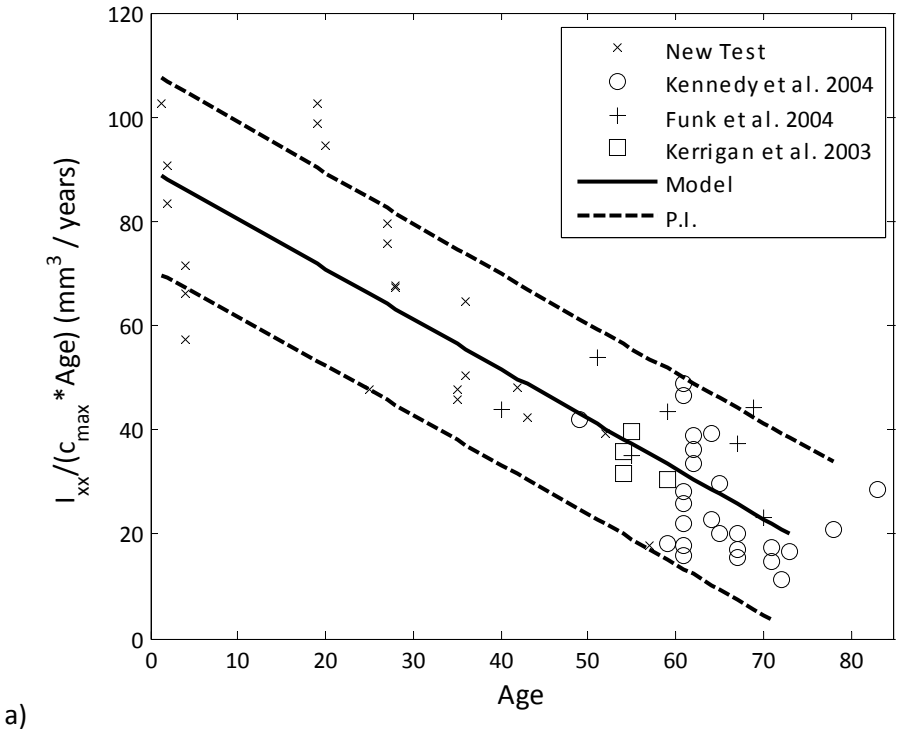

a)

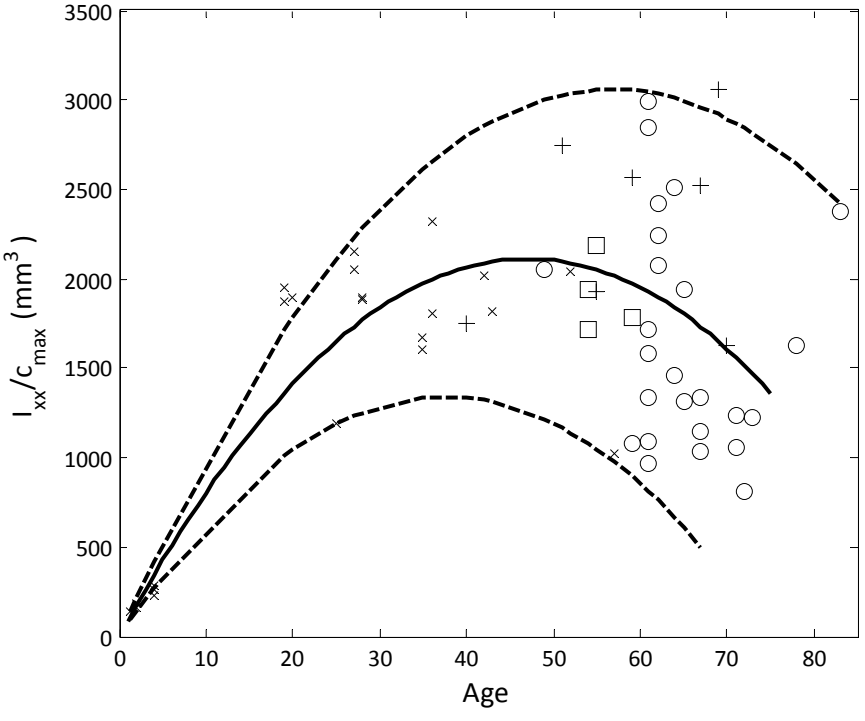

b)

Figure 4: The section modulus, I_{xx}/c_{max}, versus age for the aforementioned subset of specimens (n=58 tests). Top: I_{xx}/c_{max} values normalized by age, with a linear model and an 85% prediction interval (P.I.) fit to those data. Bottom: I_{xx}/c_{max} versus age, with the model and prediction bounds developed in plot (A) denormalized.

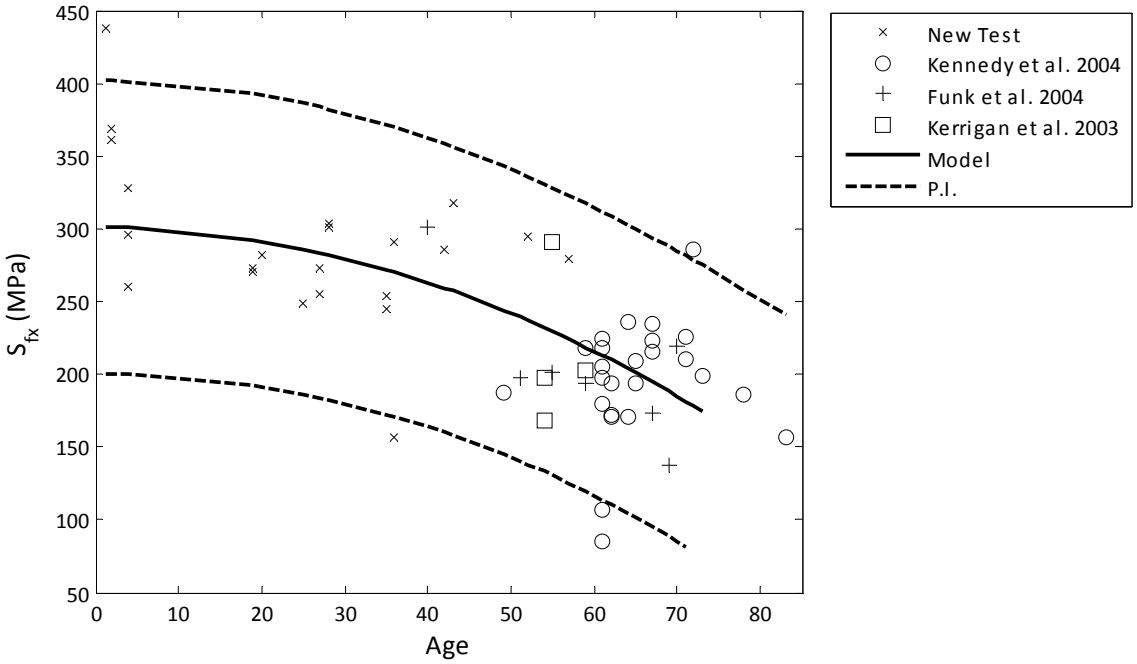

Figure 5: S_{fx} versus age for the aforementioned subset of specimens (N=58 tests), with associated model and 95% prediction interval (P.I.).

TABLE II
MODEL COEFFICIENTS (WITH 95% COEFFICIENT CONFIDENCE INTERVALS) AND MODEL R^2 VALUES

	Coefficient	Value	95% C.I	R^2
$I_{xx}/(c_{max}$xAge) v. Age	a	0.9561	(0.8073, 1.105)	0.747
	b	89.883	(81.97, 97.79)	
S_{fx} v. Age*	c	$2.371\text{x}10^{-5}$	$(1.65, 3.09)\text{x}10^{-5}$	0.439
	d	0.301	(0.277, 0.325)	
M_{fx} v. Age	A	0.7980	-- **	0.6483
	B	77.539	--	
	C	0.00002	--	
	D	0.3160	--	

* These model coefficients result in S_{fx} measured in Nm/mm^3 (necessary for combining the two component models to predict M_{fx}). Figure 5 shows the same model, multiplied by 10^3 to achieve S_{fx} in units of MPa.

** This model solution is not unique (due to multiple second-order terms in the model, Equation 11). As a result the coefficient confidence intervals approach infinity and are meaningless.

Component Analysis

Consistent with the beam equation shown in Equation 4, the mid-shaft moment at fracture followed a general linear trend with the section modulus I_{xx}/c_{max} (Figure 3). This relationship began to diverge for increasing I_{xx}/c_{max}, suggesting a gradual change in the material characteristics (or other factors) affecting the failure moment.

The section modulus I_{xx}/c_{max} exhibited a rapid increase over the first 25 years consistent with developmental bone growth. This was followed by a substantial divergence with inter-subject variation, with a decreasing trend with greater age (Figure 4b). This divergence and decreasing trend with age is consistent with mechano-physiological processes of bone remodeling. Throughout development, the mean diameter of the hollow cylinder made by cortical bone gradually increases through a process of periosteal deposition on the outer

surface, accompanied by circumendosteal resorption reclaiming bone from the interior surface [2]. The periosteal deposition process slows at skeletal maturity. Depending on various factors, the endosteal resorption process can either slow correspondingly to the point of equilibrium, or can continue through advanced age [2]. In the case of continuing endosteal resorption, this may cause an overall thinning of the cortical bone resulting in a decrease in I_{xx}/c_{max}. The nature and magnitude of this bone remodeling is likely dependent on the loading applied to the femur throughout life [2], consistent with the increasing variability in I_{xx}/c_{max} observed in the current study with increasing age.

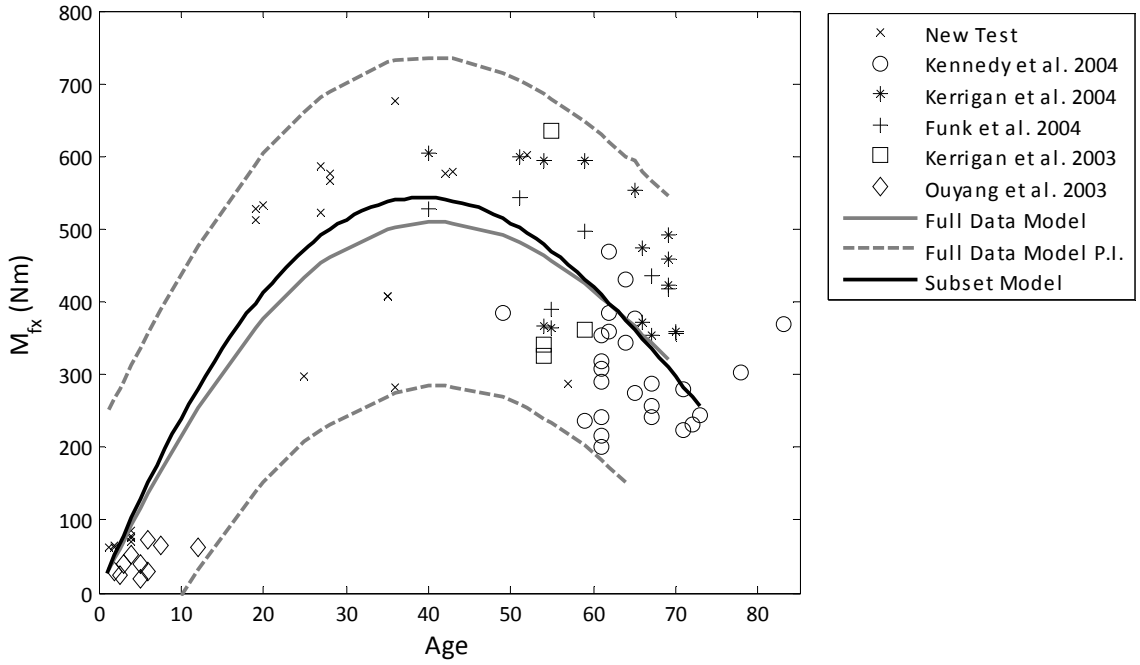

Figure 6: Fracture moment versus age for the entire dataset, compared to the model generated by combining the component ("subset") models shown in Figure 4 and Figure 5. Also shown is a model of similar form fit to the entire set of data ("full data model"), with the corresponding 95% prediction interval (P.I.).

The remainder term, S_{fx}, tended to be relatively consistent for the first 40 years followed by a decline. This is generally consistent with previously reported trends on the relation between the ultimate tensile stress of femur cortical bone and age. Yamada et al. [3] describes ultimate tensile strength values for human femoral bone that are relatively consistent from ages 10-49 years, followed by a gradual decline with increasing age. Lindahl and Lindgren [4] observed a decreasing trend in the ultimate tensile stress in femur cortical bone throughout the entirety of adulthood (approximately age 15-89). Due to a dearth of information it is difficult to compare the S_{fx} results to trends in σ_{ult} for younger ages. The limited studies available suggest various trends for σ_{ult} through infancy and adolescence, indicating either slightly lower [24], [14] or considerably lower [25] σ_{ult} values for very young (infant) pediatric specimens relative to adults. The observation that S_{fx} tended to be greatest for the youngest specimens in this study may indicate a contribution from other material or morphological differences between developing and adult bone, such as fracture toughness [26], [9], [6] or porosity [5], [6], [7], [8].

Although the trends with age were generally similar, the magnitude of S_{fx} tended to vary over a substantially greater range than typical values of femur bone ultimate tensile stress reported in the literature. The values for S_{fx} calculated here ranged from approximately 75-440 MPa. In contrast, reported values for femur cortical bone ultimate tensile stress tend to vary from 55.7-200 MPa [25], [3]. This suggests that S_{fx} does not solely represent the ultimate stress of the tissue, but likely incorporates other factors affecting the occurrence of fracture. This may include the density or size of inhomogeneities (porosity, etc.) that may act as initiation sites for crack propagation [11], [6]. This may also be the result of differences in strain rates between previous material property tests and the bending tests presented here [27].

Models

The model generated from combining the subset component analyses was relatively consistent with the trends observed in the whole dataset (Figure 6). The component model differed from the model generated by the whole dataset by only 6% at the peak. This suggests that, when combined, the component models resulted in a reasonable description of the overall relationship between the mid-shaft fracture moment and age observed in the whole dataset. This also supports the supposition that the trends observed in the subset regarding I_{xx}/c_{max} and S_{fx} may be consistent in the larger dataset.

Practical Implications

This is the first study (to the authors' knowledge) to quantitatively relate changes in long-bone fracture tolerance with age to contributing mechanistic factors. This work was performed without any pre-conceptions regarding similarities or dissimilarities between bone mechanics of different age groups. Age itself does not necessarily contribute causally to changes in skeletal fracture tolerance. Instead, skeletal fracture tolerance is related to mechanistic geometric and material factors that change throughout skeletal development and subsequent periods, which may be roughly correlated to age (with substantial interpersonal variations). This study suggests that the femur fracture tolerance to mid-shaft, 3-point bending increases through skeletal development, followed by a peak or a plateau, followed by a decline with advanced age. The results suggest that the initial increase in fracture tolerance during skeletal development is the result of increases in the cross-sectional geometric factors that resist bending (I_{xx}/c_{max}). The decline with advanced age appears to result from a decrease in the geometric section modulus, accompanied by a decrease in other factors that affect fracture risk (which likely includes, but is not limited to, a decrease in the ultimate stress of the cortical bone). The descriptive models developed here provide an understanding of the relationship between those geometric factors, remaining factors, and fracture moment with age. This may facilitate improved prediction of femur fracture risk not only with age, but also when targeting specific subject characteristics, anthropometries, or pathologies which may be described within the models developed here.

Strain Rate Dependence

This study combined results from tests that used different loading rates. A majority of the tests used loading rates of 1.2-1.5 m/s. The tests of Kennedy et al. [18] used nominal loading rates of 5 m/s. The pediatric tests of Ouyang et al. [21] used nominal loading rates of 0.008 m/s (500 mm/min). Care should be taken when combining disparate tests in this manner as the mechanical properties of bone, in general, are strain rate dependent. Currey [28] estimated that the ultimate stress of cortical bone is related to the applied strain rate, $\dot{\varepsilon}$, by the following:

$$\sigma_{ult} = 177\dot{\varepsilon}^{0.067} \tag{12}$$

According to Kennedy et al. [18] and Funk et al. [19], typical average strain rates for the 5 m/s and 1.2 m/s tests were approximately 0.5 /s and 0.1 /s, respectively. Based on the model of Currey [28], this would translate into an approximately 11% difference in cortical bone ultimate stress. While this difference is non-trivial, it is small compared to the overall trends and range of data observed in this study.

Because of the non-linearity of Equation 12, it is expected that a greater strain rate effect would be observed when comparing the 0.008 m/s tests of Ouyang et al. [21] to the faster tests of the rest of the dataset. Consistent with the lower strain rate, the Ouyang et al. [21] tests exhibited fracture moments less than those observed in the new, higher-rate pediatric tissue tests (Figure 6). While this should be considered when comparing the different test series shown in Figures 2 and 6, these differences likely have little effect on the overall results of this study. Because of a lack of geometry information, the Ouyang et al. [21] tests were excluded from the mechanistic component decomposition analysis shown in Figures 3-5. Removing the Ouyang et al. [21] data also has little effect on the M_{fx} vs. *Age* model developed for the entire dataset (Figure 6), with a less than 5% change in the model peak if the 0.008 m/s tests are removed.

Limitations and Future Work

A major inter-test variation included the presence or absence of flesh. Although this was adjusted for, the

adjustment factor was derived from injury risk functions and thus represents a mean effect and does not necessarily capture differences with flesh on an individual basis.

This study also employed a simplified beam model to relate femur fracture moment to contributing mechanistic factors. This was based on the cross-sectional geometry at the mid-shaft, and assumed that the neutral bending axis passed through the area centroid perpendicular to the direction of loading. The true mechanics of fracture, however, are likely considerably more complex. The fractures in the new tests rarely initiated at the mid-shaft, commonly beginning at other locations and traveling obliquely through the bone (often resulting in a comminuted fracture). The occurrence of fracture is also likely dependent on local porosity and inhomogeneities [11], [5], [6], [7], [8]. Previous studies have also suggested that the neutral axis of femurs subjected to bending tends to shift during deformation of the bone [19]. Future work may include more detailed component-level analysis of factors contributing to femur fracture tolerance with age, possibly through subject-specific finite element (FE) modeling.

This study examined 3-point bending tests in part due to their relative abundance in the literature. 3-point bend tests are somewhat limited, however, in that they result in non-uniform bending moments throughout the length of the bone (with a peak, in this case, at the mid-shaft). Unlike other testing methods that result in uniform bending moments through a region of the bone (e.g., 4-point bending), the peak mid-shaft moment in 3-point bending is affected by the interaction between the change in applied moment along the bone combined with differences in local fracture strength. As a result the peak mid-shaft moment is an indicator of overall, structural bending strength under this loading configuration, as opposed to an indicator of local or minimum fracture tolerance. The primary goal of this study was to investigate the function of the mid-shaft cross-sectional geometry as a predictor of overall bending strength (indicated by the peak mid-shaft moment). If it is desired to study local tolerance or ultimate stress precisely, then a beam analysis similar to that presented here could be performed targeting the local moments and cross-sectional geometries at the precise locations of fracture.

V. CONCLUSIONS

This study compiled a database of 83 tests of human femurs subjected to dynamic, mid-shaft, three-point bending spanning an age range from 1.3-83 years. This included 23 new experiments to augment previous tests available in the literature. The resulting dataset exhibited a rapid increase in fracture moment throughout skeletal development up to a plateau or peak at adulthood (approximately 25-50 years), followed by a gradual decline with advanced age. The fracture moment of pediatric specimens ranged from 24-85 Nm (age 1.3 to 12 years; fracture moment adjusted for the presence of flesh during testing). The fracture moment for adult specimens ranged from 283-676 Nm for person age 20-55, compared to fracture moments ranging from 223-492 Nm for persons age ≥69 years. A component decomposition analysis was then performed for the subset of medial-lateral bending tests for which detailed geometric information was available. That analysis suggests that the increase in fracture moment during development was primarily attributable to changes in the cross-sectional bone geometry during growth. The analysis also suggests that the decrease observed with advanced age is likely due to a combination of changes in the geometry (e.g., thinning of the cortical shell) accompanied by changes in other factors affecting fracture tolerance (possibly including, but not limited to, a decrease in the ultimate stress of the cortical bone).

VI. ACKNOWLEDGEMENT

This work was supported in part by a Whitaker International Scholars grant. All new experimentation was performed at the European Center for Injury Prevention.

VII. REFERENCES

[1] Scheuer L, Black S, Christie A, Bone Development, in Developmental Juvenile Osteology, pages 18-31, *Academic Press*, London, 2000.

[2] Carter DR, van der Meulen MC, Beaupre GS, Mechanical factors in bone growth and development, *Bone*, 18, 1 Suppl, pages 5S-10S, 1996.

[3] Yamada H, Strength of Biological Materials, ed. Evans GF, *The Williams & Wilkins Company*, Baltimore,

1970.

[4] Lindahl O, Lindgren AG, Cortical bone in man. II. Variation in tensile strength with age and sex, *Acta Orthop.Scand.*, 38, 2, pages 141-147, 1967.

[5] Ural A, Vashishth D, Effects of intracortical porosity on fracture toughness in aging human bone: a microCT-based cohesive finite element study, *J.Biomech.Eng*, 129, 5, pages 625-631, 2007.

[6] McCalden RW, McGeough JA, Barker MB, Court-Brown CM, Age-related changes in the tensile properties of cortical bone. The relative importance of changes in porosity, mineralization, and microstructure, *J.Bone Joint Surg.Am.*, 75, 8, pages 1193-1205, 1993.

[7] Laval-Jeantet AM, Bergot C, Carroll R, Garcia-Schaefer F, Cortical bone senescence and mineral bone density of the humerus, *Calcif.Tissue Int.*, 35, 3, pages 268-272, 1983.

[8] Zioupos P, Ageing human bone: factors affecting its biomechanical properties and the role of collagen, *J.Biomater.Appl.*, 15, 3, pages 187-229, 2001.

[9] Wang X, Puram S, The toughness of cortical bone and its relationship with age, *Ann.Biomed.Eng*, 32, 1, pages 123-135, 2004.

[10] Nalla RK, Kruzic JJ, Kinney JH, Ritchie RO, Effect of aging on the toughness of human cortical bone: evaluation by R-curves, *Bone*, 35, 6, pages 1240-1246, 2004.

[11] Nalla RK, Kruzic JJ, Kinney JH, Balooch M, Ager III JW, Ritchie RO, Role of microstructure in the aging-related deterioration of the toughness of human cortical bone, *Materials Science and Engineering: C*, 26, 8, pages 1251-1260, 2006.

[12] Kent R, Lee SH, Darvish K, Wang S, Poster CS, Lange AW, Brede C, Lange D, Matsuoka F, Structural and material changes in the aging thorax and their role in crash protection for older occupants, *Stapp.Car.Crash.J.*, 49, pages 231-249, 2005.

[13] Wang X, Shen X, Li X, Agrawal CM, Age-related changes in the collagen network and toughness of bone, *Bone*, 31, 1, pages 1-7, 2002.

[14] Currey JD, Butler G, The mechanical properties of bone tissue in children, *J.Bone Joint Surg.Am.*, 57, 6, pages 810-814, 1975.

[15] Ivarsson BJ, Crandall JR, Longhitano DC, Okamoto M, Lateral injury criteria for the 6-year-old pedestrian - part II: criteria for the upper and lower extremities, *SAE International Congress*, 2004.

[16] Kerrigan JR, Drinkwater DC, Kam CY, Murphy DB, Ivarsson BJ, Crandall JR, Patrie J, Tolerance of the human leg and thigh in dynamic latero-medial bending, *I.J.Crash*, 9, 6, pages 607-623, 2004.

[17] Society of Automotive Engineers, J211-1 Instrumentation for impact test - part 1 - electronic instrumentation, in Surface Vehicle Recommended Practice, J211-1, *SAE International*, Warrendale, PA, 1995.

[18] Kennedy EA, Hurst WJ, Stitzel JD, Cormier JM, Hansen GA, Smith EP, Duma SM, Lateral and posterior dynamic bending of the mid-shaft femur: fracture risk curves for the adult population, *Stapp.Car.Crash.J.*, 48, pages 27-51, 2004.

[19] Funk JR, Kerrigan JR, Crandall JR, Dynamic bending tolerance and elastic-plastic material properties of the human femur, *Annu.Proc.Assoc.Adv.Automot.Med.*, 48, pages 215-233, 2004.

[20] Kerrigan JR, Bhalla KS, Madeley NJ, Funk JR, Bose D, Crandall JR, Experiments for establishing pedestrian-

impact lower limb injury criteria, *Society of Automotive Engineers Paper No.2003-01-0895*, 2003.

[21] Ouyang J, Zhu Q, Zhao W, Xu Y, Chen W, Zhong S, Biomechanical character of extremity long bones in children, *Chinese Journal of Clinical Anatomy*, 21, 6, pages 620-623, 2003.

[22] Kress TA, Porta DJ, Snider JN, Fuller PM, Fracture patterns of human cadaver long bones, *Proceedings International Research Council on the Biomechanics of Impact*, 1995.

[23] Martens M, Van AR, de MP, Mulier JC, Mechanical behaviour of femoral bones in bending loading, *J.Biomech.*, 19, 6, pages 443-454, 1986.

[24] Franklyn M, Peiris S, Huber C, Yang KH, Pediatric material properties: a review of human child and animal surrogates, *Crit Rev Biomed Eng*, 35, 3-4, pages 197-342, 2007.

[25] Hirsch C, Evans FG, Studies on Some Physical Properties of Infant Compact Bone, *Acta Orthop.Scand.*, 35, pages 300-313, 1965.

[26] Currey JD, Changes in the impact energy absorption of bone with age, *J.Biomech.*, 12, 6, pages 459-469, 1979.

[27] Currey JD, The effects of strain rate, reconstruction and mineral content on some mechanical properties of bovine bone, *J.Biomech.*, 8, 1, pages 81-86, 1975.

[28] Currey JD, Strain rate and mineral content in fracture models of bone, *J.Orthopead.Res.*, 6, pages 32-38, 1988.

VIII. APPENDIX A: FEMUR BEND DATA – ENTIRE COMBINED DATASET

TABLE AI-A

DYNAMIC MID-SHAFT FEMUR BEND TEST DATASET

Source	Age (years)	Gender	Aspect	Loading Direction*	Flesh?	I_{xx} (mm^4)	C_{max} (mm)	M_{fx} (Nm)	Adj. M_{fx} (Nm)†
Kennedy et al. 2004	61	F	NA**	M-L	Yes	25630	19.2	335	290
Kennedy et al. 2004	65	M	NA	M-L	Yes	21620	16.4	318	275
Kennedy et al. 2004	49	M	NA	M-L	Yes	41070	20.0	443	384
Kennedy et al. 2004	62	M	NA	M-L	Yes	46950	19.4	541	468
Kennedy et al. 2004	59	F	NA	M-L	Yes	14200	13.2	272	235
Kennedy et al. 2004	83	M	NA	M-L	Yes	38840	16.4	428	371
Kennedy et al. 2004	71	F	NA	M-L	Yes	13550	12.8	258	223
Kennedy et al. 2004	67	F	NA	M-L	Yes	16890	16.4	280	242
Kennedy et al. 2004	65	M	NA	M-L	Yes	28950	15.0	434	376
Kennedy et al. 2004	73	F	NA	M-L	Yes	20520	16.8	281	243
Kennedy et al. 2004	64	M	NA	M-L	Yes	27580	19.0	396	343
Kennedy et al. 2004	61	F	NA	M-L	Yes	13730	12.6	249	216
Kennedy et al. 2004	62	M	NA	M-L	Yes	40260	18.0	443	384
Kennedy et al. 2004	71	M	NA	M-L	Yes	19940	16.2	322	279
Kennedy et al. 2004	61	M	NA	M-L	Yes	52200	18.4	279	242
Kennedy et al. 2004	61	M	NA	M-L	Yes	26480	16.8	410	355
Kennedy et al. 2004	64	M	NA	M-L	Yes	42110	16.8	496	429
Kennedy et al. 2004	78	M	NA	M-L	Yes	26890	16.6	349	302
Kennedy et al. 2004	61	F	NA	M-L	Yes	12600	13.0	231	200
Kennedy et al. 2004	62	M	NA	M-L	Yes	38090	18.4	414	358
Kennedy et al. 2004	61	M	NA	M-L	Yes	50940	17.0	368	319
Kennedy et al. 2004	61	M	NA	M-L	Yes	27800	16.2	357	309
Kennedy et al. 2004	72	F	NA	M-L	Yes	12930	16.0	267	231
Kennedy et al. 2004	67	F	NA	M-L	Yes	19200	14.4	333	288
Kennedy et al. 2004	67	F	NA	M-L	Yes	17370	15.2	296	256
Kerrigan et al. 2004	66	M	R	M-L	Yes	NA	NA	548	474
Kerrigan et al. 2004	69	M	L	M-L	Yes	NA	NA	568	492
Kerrigan et al. 2004	65	M	L	M-L	Yes	NA	NA	640	554
Kerrigan et al. 2004	54	M	L	M-L	Yes	NA	NA	424	367
Kerrigan et al. 2004	69	M	R	M-L	Yes	NA	NA	488	422
Kerrigan et al. 2004	54	M	R	M-L	Yes	NA	NA	685	593
Funk et al. 2004	67	M	L	A-P	No	66518	16.5	355	--
Funk et al. 2004	59	M	R	A-P	No	70771	14.7	593	--
Funk et al. 2004	40	M	L	A-P	No	49508	15.4	605	--
Funk et al. 2004	55	M	R	A-P	No	21297	14	363	--
Funk et al. 2004	70	M	L	A-P	No	33845	13.2	359	--
Funk et al. 2004	69	M	R	A-P	No	38264	13.7	460	--
Funk et al. 2004	51	M	L	A-P	No	45506	17.1	599	--
Funk et al. 2004	66	M	R	A-P	No	22908	14.5	373	--
Funk et al. 2004	67	M	R	M-L	No	35234	14	435	--
Funk et al. 2004	59	M	L	M-L	No	42940	16.7	497	--

***** M-L = medial-lateral bending; A-P = anterior-posterior bending

** NA = Not Available

† M_{fx} multiplied by 0.866 to adjust for the presence of flesh.

TABLE AI-B
DYNAMIC MID-SHAFT FEMUR BEND TEST DATASET

Source	Age (years)	Gender	Aspect	Loading Direction*	Flesh?	I_{xx} (mm^4)	C_{max} (mm)	M_{fx} (Nm)	Adj. M_{fx} (Nm)†
Funk et al. 2004	40	M	R	M-L	No	26634	15.2	528	--
Funk et al. 2004	55	M	L	M-L	No	27008	14	389	--
Funk et al. 2004	70	M	R	M-L	No	23189	14.3	356	--
Funk et al. 2004	69	M	L	M-L	No	32075	10.5	419	--
Funk et al. 2004	51	M	R	M-L	No	39568	14.4	543	--
Kerrigan et al. 2003	55	M	L	M-L	No	29727	13.6	635	--
Kerrigan et al. 2003	59	F	R	M-L	No	24661	13.8	362	--
Kerrigan et al. 2003	54	F	L	M-L	No	27292	15.9	340	--
Kerrigan et al. 2003	54	F	R	M-L	Yes	28545	14.7	377	326
Ouyang et al. 2003‡	2	NA**	NA	A-P	No	NA	NA	29.6	--
Ouyang et al. 2003	2.5	NA	NA	A-P	No	NA	NA	24.3	--
Ouyang et al. 2003	3	NA	NA	A-P	No	NA	NA	39.6	--
Ouyang et al. 2003	4	NA	NA	A-P	No	NA	NA	51.7	--
Ouyang et al. 2003	5	NA	NA	A-P	No	NA	NA	20.4	--
Ouyang et al. 2003	5	NA	NA	A-P	No	NA	NA	40.4	--
Ouyang et al. 2003	6	NA	NA	A-P	No	NA	NA	30.4	--
Ouyang et al. 2003	6	NA	NA	A-P	No	NA	NA	73.0	--
Ouyang et al. 2003	7.5	NA	NA	A-P	No	NA	NA	65.2	--
Ouyang et al. 2003	12	NA	NA	A-P	No	NA	NA	63.5	--
New Test	36	M	L	M-L	No	27605	15.3	283	--
New Test	20	M	R	M-L	No	28247	14.9	533	--
New Test	27	M	R	M-L	No	28397	13.9	522	--
New Test	4	F	R	M-L	No	NA	NA	78.5	--
New Test	2	M	R	M-L	No	1190.6	6.57	65.5	--
New Test	43	M	R	M-L	No	27661	15.2	579	--
New Test	35	M	L	M-L	No	23576	14.1	409	--
New Test	57	F	L	M-L	No	12534	12.2	287	--
New Test	19	M	L	M-L	No	28314	14.5	528	--
New Test	52	M	R	M-L	No	29886	14.6	602	--
New Test	27	M	L	M-L	No	32765	15.3	587	--
New Test	42	M	L	M-L	No	29591	14.7	577	--
New Test	25	M	L	M-L	No	14671	12.3	297	--
New Test	28	M	L	M-L	No	27222	14.5	567	--
New Test	35	M	R	M-L	No	21476	13.4	407	--
New Test	36	M	R	M-L	No	34652	14.9	675	--
New Test	28	M	R	M-L	No	28578	15.1	577	--
New Test	19	M	R	M-L	No	26625	14.2	512	--
New Test	4	F	R	M-L	No	2215.65	7.75	84.8	--
New Test	2	M	L	M-L	No	1092.7	6.56	61.4	--
New Test	1.33	M	R	M-L	No	814.28	5.78	61.7	--
New Test	4	F	L	M-L	No	2001.3	7.55	69.1	--
New Test	4	F	L	M-L	No	1577.9	6.86	75.5	--

***** M-L = medial-lateral bending; A-P = anterior-posterior bending

** NA = Not Available

† M_{fx} multiplied by 0.866 to adjust for the presence of flesh.

‡ Data from Ouyang et al. obtained via the citing publication, Ivarsson et al. 2004 [15]